

Characterization of Pipe-Flow Turbulence and Mass Transfer in a Curved Swirling Flow Behind an Orifice

N. Fujisawa, R. Watanabe, T. Yamagata and N. Kanatani

Abstract This paper deals with the extraction of turbulent structure correlated with the wall mass transfer in a curved swirling pipe flow behind an orifice. The cross-sectional velocity field behind the orifice is measured by the Stereo Particle Image Velocimetry (SPIV) and the results are analyzed by the proper orthogonal decomposition (POD). The instantaneous velocity field shows the asymmetric vortex structure in the cross section due to the combined effect of the swirling flow and the secondary flow generated at the upstream elbow. The POD analysis indicates that the highly turbulent flow is generated on the upper left-hand side of the pipe in the lower POD modes suggesting the occurrence of high wall-thinning rate due to the mass transfer enhancement, while that of the higher modes do not show such asymmetry. This result suggests that the lower POD modes of the velocity field contribute to the non-axisymmetric pipe-wall thinning behind an orifice in a curved swirling flow.

1 Introduction

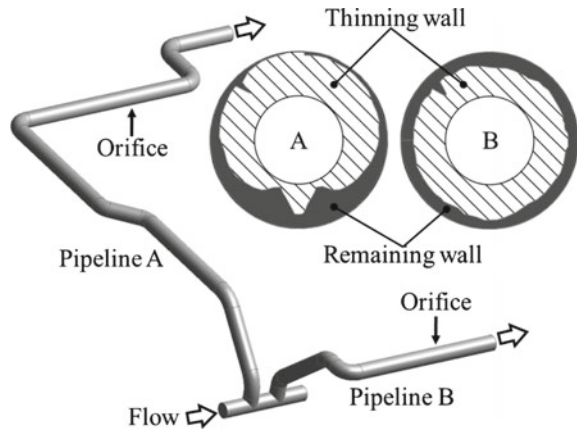
Pipe-wall thinning due to the flow accelerated corrosion (FAC) is one of the important issues in the safety management of the steel pipeline in the nuclear/fossil power plant. The mechanism of FAC is the corrosion of the wall materials of the pipeline, which is accelerated by the turbulence in the flow field, while it is also influenced by the chemical aspect of the fluid, such as temperature, pH, oxygen concentration, and so on [4]. Such complex phenomenon of FAC often occurs in the pipe wall behind the orifice, T-junction, and in the elbow, where the turbulence is highly generated by the flow separation and the related flow phenomenon [10].

N. Fujisawa (✉) · T. Yamagata
Visualization Research Center, Niigata University, Niigata, Japan
e-mail: fujisawa@eng.niigata-u.ac.jp

T. Yamagata
e-mail: yamagata@eng.niigata-u.ac.jp

R. Watanabe · N. Kanatani
Graduate School of Science and Technology, Niigata University, Niigata, Japan

Fig. 1 Illustration of pipeline geometry



Non-axisymmetric pipe-wall thinning due to FAC is a topic of interest, since the pipeline break accident in the Mihama nuclear power plant in 2004 [14]. The pipeline layout consists of an elbow, a straight pipe, and an orifice, as shown in Fig. 1. The pipeline break happened at one diameter downstream of the orifice. It should be mentioned that the swirling flow was observed in the scaled model experiment [14]. The resulting wall thinning rate was not uniform in the circumferential direction, which accelerated the pipeline accident. Since then, several studies have been carried out to elucidate the mechanism of the non-axisymmetric pipe-wall thinning due to FAC. Ohkubo et al. [15] and Fujisawa et al. [6] indicate the influence of orifice bias on the non-axisymmetric pipe-wall thinning and Takano et al. [20] suggest the influence of the elbow, but the main cause of the non-axisymmetry has not been fully understood yet due to the complexity of the flow field and the related mechanism of FAC in the actual pipelines. To understand the flow mechanism of non-axisymmetric pipe-wall thinning, the velocity field behind the orifice has been measured by the stereo PIV, which allows the three components of instantaneous velocity field in the two-dimensional cross section of interest [7]. The results indicate that the mean velocity field and the turbulent energy distribution become non-axisymmetric, suggesting the correlation of the flow field and the mass transfer. In the past, the flow parameters, such as the vertical velocity [10], turbulent energy [19, 22, 23], and wall shear stress [21] are considered as major parameters contributing to the wall mass transfer [17, 20], but the structure of turbulence has not been identified yet in literature.

Proper orthogonal decomposition (POD) is one of the statistical methods for analyzing the low-dimensional representation of the multidimensional flow field of interest. The snapshot POD is very useful for recognizing the coherent structure of turbulent flow [2]. There are several successful examples of the snapshot POD analysis applied to the turbulent flow in the literature, such as the jet in counter flow [3], channel flow [13], backward-facing step flow [12], complex unsteady flow [1, 9], and so on. By introducing the POD analysis, the most energetic structure of the flow has been extracted from the planar PIV data by decomposing the fluctuating

properties of the turbulent velocities into the linear sum of orthogonal eigenfunctions of temporal and spatial correlations.

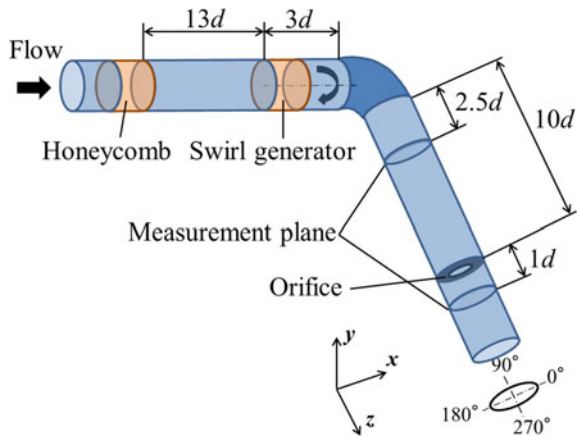
The purpose of this paper is to introduce the snapshot POD analysis into the velocity field measured by stereo PIV to localize the high mass transfer rate in the pipe wall behind an orifice under the influence of swirling flow combined with the elbow.

2 Experimental Method

2.1 Experimental Setup

The experiment on the velocity field behind an orifice in a curved swirling flow has been carried out in a closed-circuit water tunnel [6]. The water tunnel used in this experiment consists of a pump, settling chamber, honeycomb, flow-developing section, and test section of the pipeline, which have been described in [6]. The measurements of velocity field and mass transfer rate are carried out by using the stereo PIV and benzoic acid dissolution methods, respectively. Figure 2 shows the details of the test section, which consists of a swirl generator, elbow, straight pipe, orifice, and downstream pipe. It should be mentioned that the length of the straight pipe between the elbow and the orifice is set to $10d$ to meet with the Mihama case [14], where d is a pipe diameter. The diameter of the pipe is $d = 56\text{mm}$ and the radius to diameter ratio of the elbow is 1.4. The test section is made of an acrylic resin material for flow visualization. The swirling flow was generated by a swirl generator, which is made of 6 plane vanes having an angle of 45° to the flow axis [6]. The swirl generator was placed $13d$ downstream of the honeycomb and $3d$ upstream of the elbow. It should be mentioned that the swirl generator produces a swirl flow

Fig. 2 Details of experimental test section

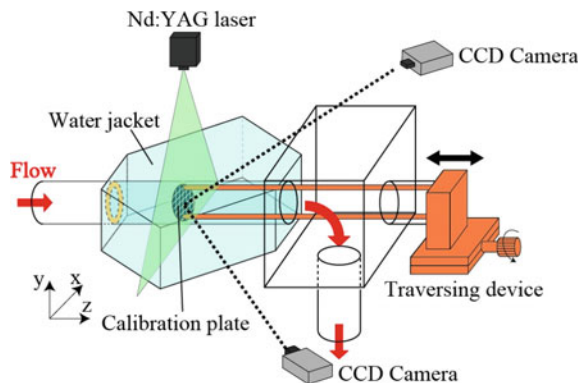


having a swirl intensity S defined by the circumferential momentum to axial one $S = 0.35$ at 3 diameters upstream of the orifice [5], while it is estimated as $S = 0.26$ in the Mihama case from the velocity measurement in the scaled model experiment [14]. In the downstream of the elbow, the straight pipe section of $10d$ and the circular orifice having a diameter ratio 0.6 are placed before entering into the downstream pipe. Note that the diameter ratio of the orifice agrees with that of the Mihama case [14]. The working fluid of water is kept at 298 K during the experiment. Therefore, the Reynolds number of the flow was set to $Re(=Ud/\nu) = 3 \times 10^4$, while that of the Mihama case was $Re = 5.8 \times 10^6$ [14], where U is the bulk velocity and ν is the kinematic viscosity of water.

2.2 Measurement of Velocity Field

The velocity field behind the orifice in the pipeline under the influence of curved swirling flow was measured by the stereo PIV system, which can measure the three-dimensional velocity field in the cross section of interest using the two oblique observations through the water jackets on both sides of the pipe. Figure 3 shows an illustration of the experimental test section and the stereo PIV system for the three-dimensional velocity measurement. The stereo PIV system consists of two CCD cameras with the frame straddling function (1018×1008 pixels with 8 bits in gray level), double pulsed Nd:YAG lasers (maximum output power 50 mJ/pulse), and a pulse controller. The light sheet illumination for flow visualization was provided from the top of the test section normal to the pipe axis. The thickness of the light sheet was about 2 mm. The flow visualization was carried out using nylon tracer particles $40 \mu\text{m}$ in diameter having a specific gravity of 1.02, which was supplied to the flow in the tank located upstream of the pump. The two CCD cameras are located on both sides of the pipe in a Scheimpflug configuration.

Fig. 3 Stereo PIV system



The stereo PIV analysis of the two sequential images requires the calibration in a three-dimensional thin volume of interest in the light sheet plane. The calibration plate was traversed axially using the mechanical traversing gear driven manually and allowed the out-of-plane displacement of 0.5 mm in interval with an accuracy of 5 μm. Then, a total of 5 images are captured in an axial distance of 2 mm. These calibration images were used for the three-dimensional reconstruction for stereo PIV [8, 18]. The interrogation between the sequential two images was carried out using the direct cross-correlation algorithm with the sub-pixel interpolation technique. Then, the particle displacements from each camera were combined to produce the three-dimensional velocity vectors by solving the system equations for stereo cameras with a least square method. It should be mentioned that the interrogation window size was set to 31 × 31 pixels with 50% overlap in the analysis [11]. The details of the stereo PIV analysis can be found in Raffel et al. [16].

2.3 Proper Orthogonal Decomposition Analysis

The snapshot POD analysis is introduced into the statistical analysis of 1000 instantaneous velocity fields in the curved swirling flow, which is measured by stereo PIV at one diameter downstream of the orifice. The basic idea of snapshot POD is that it yields a set of orthogonal eigenfunctions that are optimal in energy representing temporal and spatial correlations of instantaneous velocities. It is assumed that the instantaneous velocity vector $U(x, t_k)$ is acquired at time t_k , where $k = 1, 2, \dots, M$. The POD analysis allows the evaluation of the mean velocity field (0th POD mode) and the fluctuating velocity field (1st, 2nd, ...). In the POD analysis, three velocity components u, v, w are arranged in the velocity matrix U and the two-point correlation matrix C_{jk} is expressed by the velocity matrix U as follows:

$$C_{jk} = \frac{1}{M} \int U(x, t_j)U(x, t_k)dx \quad (j, k = 1, 2, \dots, M) \tag{1}$$

The POD mode Φ_k is obtained by solving the following eigenvalue problem of the two-point correlation matrix C_{jk} ,

$$C_{jk}a = \lambda_k \tag{2}$$

where a is the eigenvector and λ_k is the eigenvalue of C_{jk} . The eigenvectors and eigenvalues can be obtained by solving these equations numerically.

The POD mode Φ_k can be expressed by the linear combination of the eigenvector a and the instantaneous velocity vector U , as follows:

$$\Phi_k(x) = \sum_{k=1}^N a_n^k U(x, t_k) \tag{3}$$

The fluctuating energy E_k of the corresponding POD mode is expressed by the eigenvalue λ_k divided by the total fluctuating energy E_t , which is written as follows:

$$E_k = \frac{\lambda_k}{E_t} \quad (4)$$

where

$$E_t = \sum_{k=1}^N \lambda_k = \int U(x, t_k)^2 dx \quad (5)$$

The reconstructed velocity field can be expressed by using the eigenfunction and eigenvector as follows:

$$\tilde{U}(x, t_k) = \sum_{n=1}^{N_{POD}} a_k^n \Phi_k(x) \quad (6)$$

where N_{POD} is the number of POD mode. The details of the snapshot POD analysis have been described in the literature [1–3, 12, 13]. It should be mentioned that sufficiency of the number of PIV data for the analysis was confirmed by the analysis with a small number of PIV data of 500.

3 Results and Discussions

Figure 4 shows the first three POD modes of the flow behind the orifice in a curved flow without swirl. The 0th mode (a) corresponds to the mean flow, while the 1st mode (b) and 2nd mode (c) show the fluctuating velocity fields. The 0th mode of the analysis agrees with that of the mean velocity field, which suggests the validity of the present analysis. On the other hand, the periodic pattern appears in circumferential direction in the fluctuating velocity modes. The energy levels of the 1st and 2nd POD modes are 3.8 and 3.6 %, respectively. The 1st POD mode shows the periodic pattern on the left-hand side and the 2nd POD mode shows the similar pattern on the lower side. These results indicate that the total energy of the periodic pattern is distributing almost uniformly in energy in the cross section of the pipe, suggesting the presence of axisymmetric flow structure in the pipe flow behind the curved flow.

Figure 5 indicates the corresponding three POD modes of the flow behind a curved swirling flow. The 0th POD mode shows the high axial velocity on the left-hand side of the pipe center and the high circumferential velocity on the left-hand pipe wall, suggesting the occurrence of non-axisymmetric flow behind the orifice. This flow pattern suggests the presence of a secondary flow in the pipe. On the other hand, 1st and 2nd POD modes show the presence of positive and negative sign in the cross-sectional distribution of fluctuating velocities, while the magnitude of the POD mode decreases with an increase in the mode number. The energy levels of the 1st and 2nd POD modes are 13 and 7.4 %, respectively. It should be mentioned that the presence

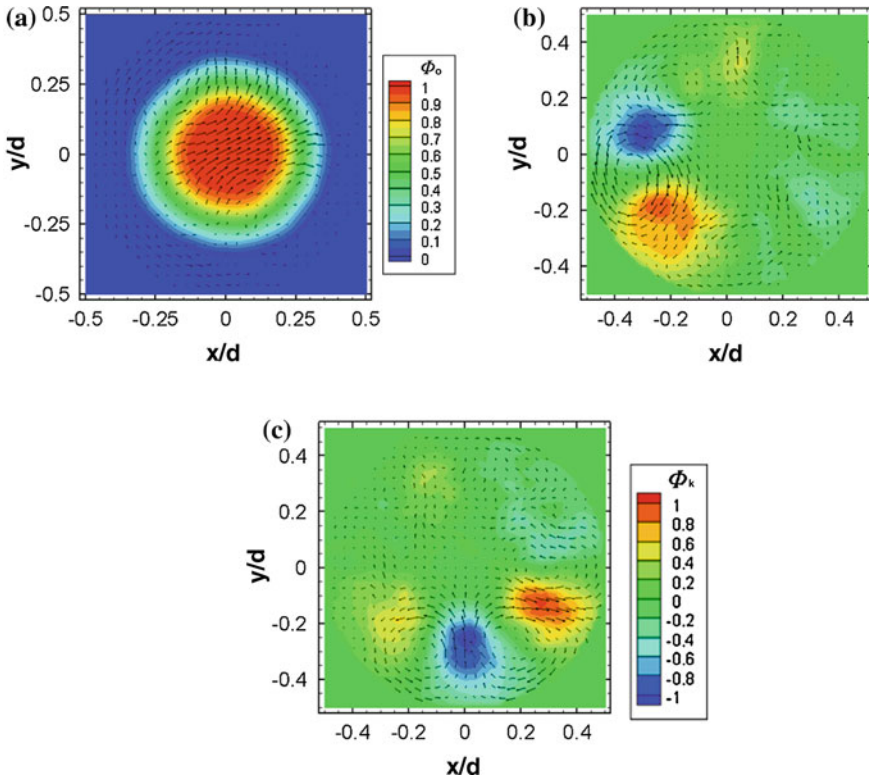


Fig. 4 Cross-sectional distributions of POD analysis without swirl. **a** Mean velocity. **b** 1st mode. **c** 2nd mode

of positive and negative sign in the neighborhood of the pipe center indicates the formation of vortex structure in the pipe. These results show the complexity of the mean and fluctuating velocity field downstream of the orifice under the influence of curved swirling flow.

Figure 6 shows the cross-sectional turbulent energy contours downstream of the orifice, which are reconstructed from the velocity field from the first 19 POD modes (a) and that from the rest of the POD modes (b). Note that the first 19 modes occupy 50% of the total energy and the rest of the POD modes the other 50%. The results indicate that the reconstructed turbulent energy by the first 19 modes shows non-axisymmetric distribution along the pipe wall and the magnitude of turbulent energy is high on the upper side and is low on the right-hand side, while the reconstructed turbulent energy contour in the rest of POD modes shows almost uniform along the wall. This result suggests that the non-axisymmetric feature of the turbulent energy in the pipe comes from the lower POD modes, which contains the high turbulent energy.

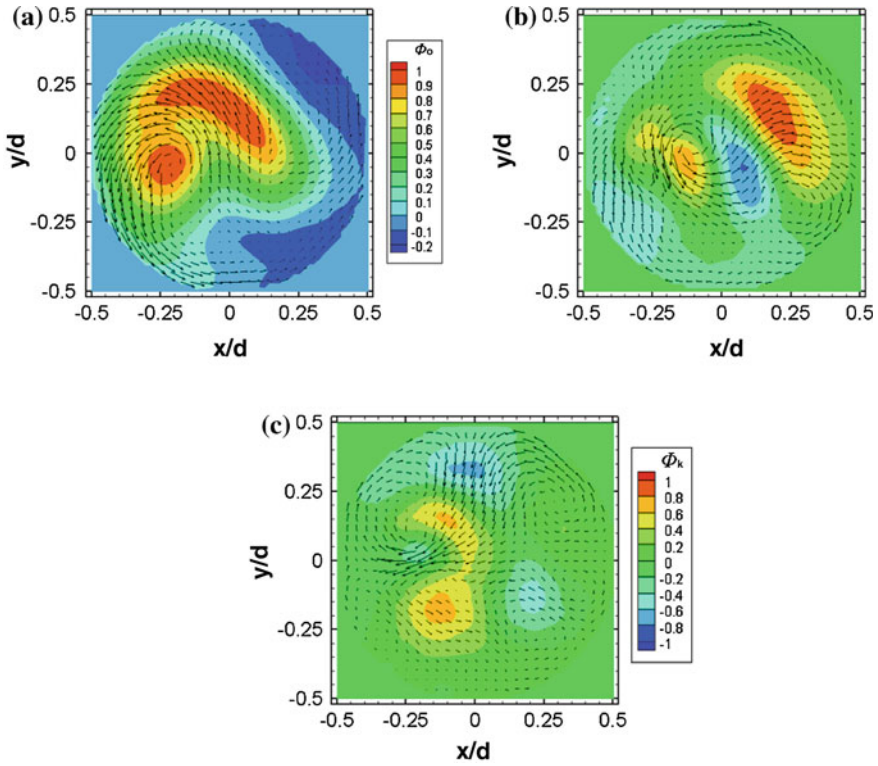


Fig. 5 Cross-sectional distributions of POD analysis with swirl. **a** Mean velocity. **b** 1st mode. **c** 2nd mode

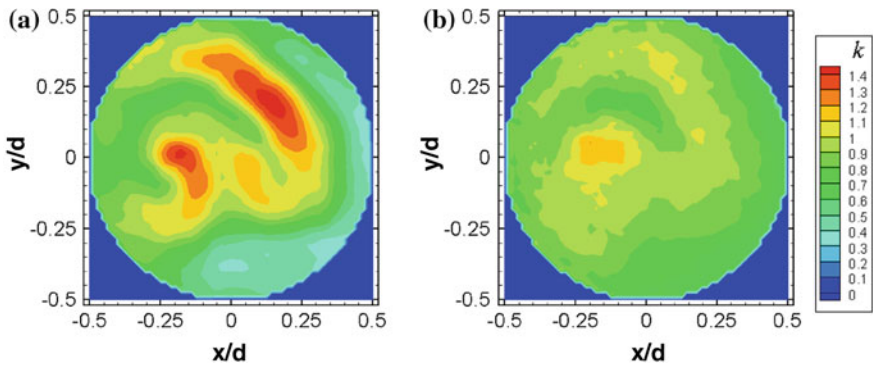


Fig. 6 Reconstruction of turbulent energy with swirl. **a** Lower POD modes. **b** Higher POD modes

Fig. 7 Distributions of wall mass transfer rate and turbulent energy

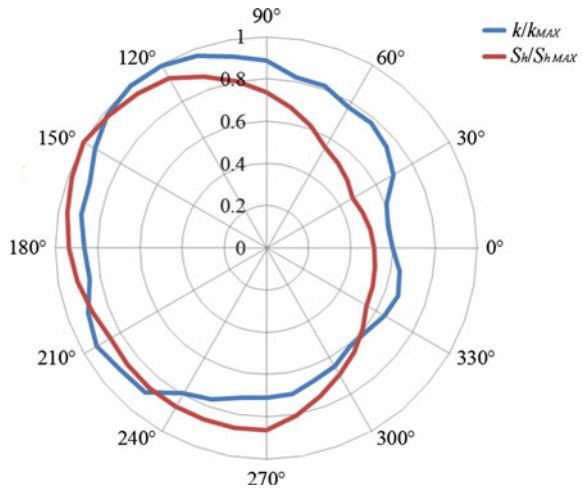


Figure 7 compares the distributions of turbulent energy k reconstructed from the velocity in lower POD modes and the mass transfer rate S_h along the pipe wall in the curved swirling flow, which is measured by the benzoic acid dissolution method [20]. They are normalized by maximum value. The result indicates that the high mass transfer rate is found on the top left side of the pipe and both results are consistent with each other. This result suggests that the turbulent energy distribution in the lower POD modes is highly correlated with that of the mass transfer rate.

4 Conclusions

The cross-sectional velocity field behind an orifice under the influence of curved swirling flow was measured by Stereo Particle Image Velocimetry, and the results were analyzed by the proper orthogonal decomposition to extract the turbulent structure correlated with the wall mass transfer. The instantaneous velocity field showed the vortical structure due to the swirling flow combined with the secondary flow caused by the upstream elbow, which is generated by non-axisymmetric flow field behind the orifice. The POD analysis showed the variation of turbulent structure in the lower POD modes due to the influence of the curved swirling flow. The turbulent energy reconstructed from the lower POD modes indicates the similar distribution to that of the mass transfer rate. This result suggests the correlation of turbulent energy in the lower POD modes with the mass transfer rate.

References

1. P. Aranyi, G. Janiga, K. Zahringer, D. Thevenin, Analysis of different POD methods for PIV; measurements in complex unsteady flows. *Int. J. Heat Fluid Flow* **43**, 204–211 (2013)
2. G. Berkooz, P. Holmes, J.L. Lumley, The proper orthogonal decomposition in the analysis of turbulent flows. *Annu. Rev. Fluid Mech.* **25**, 539–575 (1993)
3. S. Bernero, H.E. Fielder, Application of particle image velocimetry and proper orthogonal decomposition on the study of a jet in counterflow. *Exp. Fluids* **29**, S274–S281 (2000)
4. R.B. Dooley, Flow-accelerated corrosion in fossil and combined cycle/HRSG plants. *Power Plant Chem.* **10**, 68–89 (2008)
5. M. Escudier, Vortex breakdown, observations and explanations. *Prog. Aerosp. Sci.* **25**, 189–229 (1988)
6. N. Fujisawa, T. Yamagata, S. Kanno, A. Ito, T. Takano, The mechanism of asymmetric pipe-wall thinning behind an orifice by combined effect of swirling flow and orifice bias. *Nucl. Eng. Des.* **252**, 19–26 (2012)
7. N. Fujisawa, T. Yamagata, T. Takano, N. Kanatani, K. Iwata, A. Ishizuka, Experimental and numerical study on pipe-wall-thinning by swirling flow through complex pipeline geometry, in *Proceedings of 12th Asian Symposium on Visualization*, Tainan, Taiwan, ASV12-K3 (2013)
8. S. Funatani, N. Fujisawa, Simultaneous measurement of temperature and three velocity components in planar cross section by liquid-crystal thermometry combined with stereoscopic particle image velocimetry. *Meas. Sci. Technol.* **13**, 1197–1205 (2002)
9. L. Graftieaux, M. Michard, N. Grosjean, Combining PIV, POD and vortex identification algorithms for the study of unsteady turbulent swirling flows. *Meas. Sci. Technol.* **12**, 1422–1429 (2001)
10. K.M. Hwang, T.E. Jin, K.H. Kim, Identification of relationship between local velocity components and local wall thinning inside carbon steel piping. *J. Nucl. Sci. Technol.* **46**, 469–478 (2009)
11. M. Kiuchi, N. Fujisawa, S. Tomimatsu, Performance of PIV system for combustor flow and its application to spray combustor model. *J. Vis.* **8**, 269–276 (2005)
12. J. Kostas, J. Soria, M.S. Chong, A comparison between snapshot POD analysis of PIV velocity and vorticity data. *Exp. Fluids* **38**, 146–160 (2005)
13. Z.-C. Liu, R.J. Adrian, T.J. Hanratty, Large-scale modes of turbulent channel flow: transport and structure. *J. Fluid Mech.* **448**, 53–80 (2001)
14. NISA, Secondary piping rupture accident at Mihama power station, unit 3, of the Kansai Electric Power Company, Inc. (2005)
15. M. Ohkubo, S. Kanno, T. Yamagata, T. Takano, N. Fujisawa, Occurrence of asymmetrical flow pattern behind an orifice in a circular pipe. *J. Vis.* **14**, 15–17 (2011)
16. M. Raffel, C. Willert, J. Kompenhans, *Particle Image Velocimetry*, vol. 174 (Springer, Heidelberg, 1998)
17. F. Shan, A. Fujishiro, T. Tsuneyoshi, Y. Tsuji, Effects of flow field on the wall mass transfer rate behind a circular orifice in a round pipe. *Int. J. Heat Mass Transf.* **73**, 542–550 (2014)
18. S.M. Soloff, R.J. Adrian, Z.C. Liu, Distortion compensation for generalized stereoscopic particle image velocimetry. *Meas. Sci. Technol.* **8**, 1441–1454 (1997)
19. T. Sydberger, U. Lotz, Relation between mass transfer and corrosion in a turbulent pipe flow. *J. Electrochem. Soc.* **129**, 276–283 (1982)
20. T. Takano, T. Yamagata, Y. Sato, N. Fujisawa, Non-axisymmetric mass transfer phenomenon behind an orifice in a curved swirling flow. *J. Flow Control Meas. Vis.* **1**, 1–5 (2013)
21. Y. Utanohara, Y. Nagaya, A. Nakamura, M. Murase, Influence of local flow field on flow accelerated corrosion downstream from an orifice. *J. Power Energy Syst.* **6**, 18–33 (2012)

22. T. Yamagata, A. Ito, Y. Sato, N. Fujisawa, Experimental and numerical studies on mass transfer characteristics behind an orifice in a circular pipe for application to pipe-wall thinning. *Exp. Therm. Fluid Sci.* **52**, 239–247 (2014)
23. K. Yoneda, R. Morita, M. Satake, I. Inada, Quantitative evaluation of effective factors on flow accelerated corrosion (part 2), Modelling of mass transfer coefficient with hydraulic features at wall. CRIEPI Research Report, No. L07015 (2008) pp. 1–33